JOURNAL OF MATERIALS SCIENCE 28 (1993) 5508–5513

Effects of B^+ and Cr^+ ion implantation on the oxidation of Ni_3Al

CHEN MEI, S. PATU, SHI CHANGXU, SHEN JIANIAN*
Laboratory of Fatigue and Fracture for Materials, Institute of Metal Research, and **Institute of Corrosion and Protection of Metals, Academia Sinica, Shenyang 110015, People's Republic of China*

Ni_3Al samples were implanted with different doses of 150 keV B^+ and Cr^+ ions to modify the surface region and the high-temperature oxidation behaviour was tested. The surface layer structure was investigated by Auger electron spectroscopy, and transmission electron microscopy, secondary ion mass spectroscopy and optical microscopy before and after testing. The experimental results show that boron atoms exist in the form of interstitial atoms. No evidence was found that any new phase existed in boron implanted Ni_3Al. Implanted Ni_3Al alloy has better oxidation resistance than the unimplanted ones at 900 °C. For B^+-implanted Ni_3Al, the oxide layer is basically composed of fine-grained NiO inner layer and an a-Al_2O_3 outer layer. Boron is oxidized into B_2O_3 of comparatively larger grain size. B_2O_3 particles are enriched at grain boundaries and defects. This curtails the short-circuit transportation of oxygen and improves the oxidation resistance of Ni_3Al. Implantation with Cr^+ and B^+ combines the good effects of both elements and produces a remarkable improvement on the oxidation resistance. The effects of implanted elements and the possible reaction mechanisms are discussed.

1. Introduction

Ion implantation is regarded as an effective process in the surface modification of materials. Surface-related properties, such as hardness, fatigue, friction, wear and oxidation at high temperature, can be significantly improved by this technique. Ion implantation is also a new and effective tool for studying the relationship between microstructure, composition and properties of materials. Since Aoki and Izumi [1] found that small quantities of boron could improve the plasticity of Ni_3Al significantly, much interest has been centred on Ni_3Al for which brittleness has been the most formidable obstacle to fabrication and use. Scientists have achieved many results in various fields in the past 10 years [2] and the results show clearly that this intermetallic compound has many remarkable properties. In particular, the studies concerning the high-temperature oxidation behaviour of implanted Ni_3Al predicted that Ni_3Al has a good prospect as a superalloy. Because of the above-mentioned reasons and these study results, the oxidation resistance of Ni_3Al should be improved further. Therefore, it is useful to study the effects of ion implantation on the oxidation behaviour of Ni_3Al in order to give a more extensive understanding of and an increase in the knowledge concerning the practical value of the alloy.

Chromium is a normal addition to superalloys. Boron is another necessary addition to Ni_3Al to promote its unique effects. By implanting B^+ and Cr^+ ions into Ni_3Al, we aimed to study the microstructure of oxidized implanted Ni_3Al and discuss the effects of ion implantation on the oxidation behaviour of Ni_3Al.

2. Experimental procedures

A columner crystalline Ni_3Al rod, which was more ductile than polycrystalline Ni_3Al, was obtained by a directional growth technique. The growth direction determined by X-ray diffraction (XRD), was mainly [2 2 0]. The rod was annealed in a vacuum for 5 h at 1200 °C. The atomic composition is $Ni_{75.2}Al_{24.8}$ given by chemical analysis. Samples (10 mm × 10 mm × 0.5 mm) were cut vertically and in parallel from the rod and polished mechanically. The final polishing was done using 0.5 μm diamond paste. Fig. 1 shows the grain-boundary morphologies of the samples after etching in a 50% thick hydrochloric acid–50% hydrogen peroxide solution. Implantations were performed on both sides at 150 keV with different doses. Ion-implantation parameters are listed in Table I. During implantation, samples were attached using conducting cement to freon-cooled sinks.

Auger electron spectroscopy (AES) was employed to analyse the depth profile of the elements after implantation. Mass gain measurements during oxidation were performed with a recording thermobalance in static air at 900 °C. Mass changes were monitored continuously with a sensitivity of ± 0.01 mg. Observation of morphology and microstructure of the surface region was carried out on a transmission electron

0022–2461

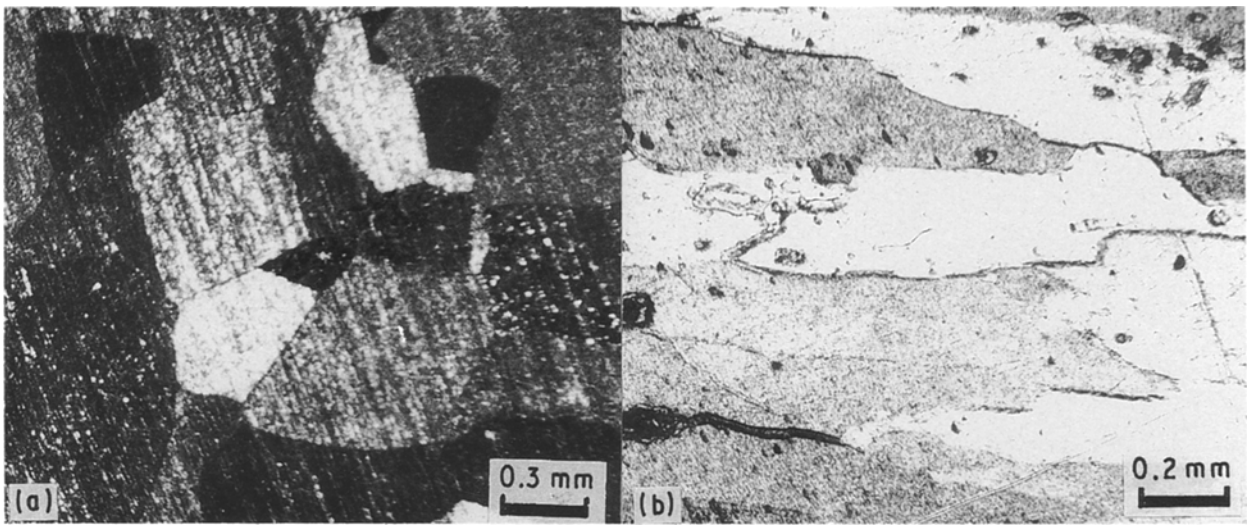

Figure 1 The morphologies of grain boundaries of Ni_3Al; (a) top view, (b) side view.

TABLE I Ion implantation test parameters

Implanted elements	Doses (ions cm^{-2})	Beam energy (keV)
B^{+a}	4×10^{16}	150
(‖)[b]	1.5×10^{17}	150
Cr^+ +	2×10^{17} +	150
B^+	1.5×10^{17}	150

[a] Top-view sample.
[b] Side-view sample.
Henceforth, unless noted to the contrary, we refer to the top-view sample.

microscope (TEM), Philips EM420, before and after oxidation. The thin films for TEM were made by the parallel method: the implanted surface was protected and ground mechanically from the other side to a thickness of about 30 μm. Then, the film was thinned from the unimplanted side by an ion-sputtering process until a hole appeared at the centre. The accelerating voltage was 4–5 keV and the argon-ion beam was at an angle of 17°.

3. Results

3.1. The surface structure of implanted Ni_3Al

Results of the AES analysis are shown in Fig. 2, which shows the depth profiles of the elements. Argon ions were used as sputter ions. The results indicate that the implanted elements are in Gaussian distributions in the matrix. A characteristic of combined implanted samples is that boron and chromium are distributed at different depths. The mixed region is very narrow. That is, there are basically two independent implanted layers in the combined implanted sample. TEM analysis showed that no new phase existed in the boron-implanted sample.

3.2. Oxidation kinetics and structure of the oxide film

3.2.1. Oxidation kinetics

Mass gain measurements of implanted and unimplanted samples at 900 °C in air at 1 atm, revealed an

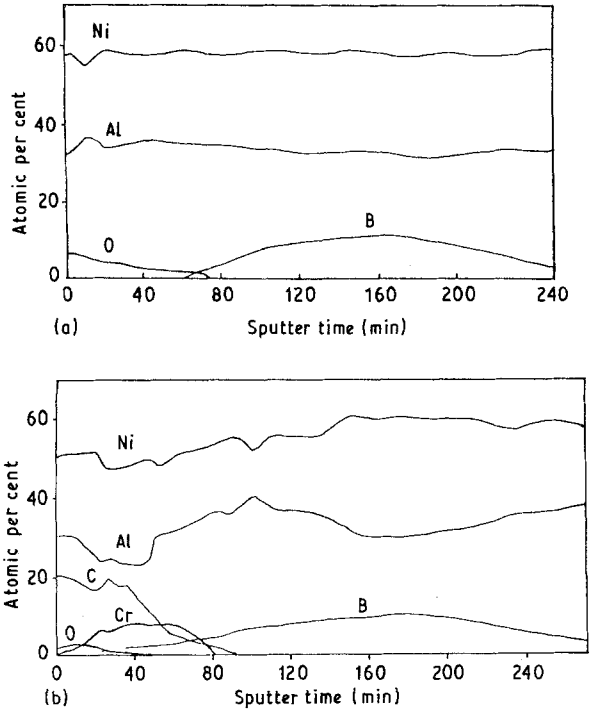

Figure 2 Auger depth profiles of (a) B^+ (1.5×10^{17} ions cm^{-2}), (b) Cr^+ (2×10^{17} ions cm^{-2}) + B^+ (1.5×10^{17} ions cm^{-2})-implanted Ni_3Al.

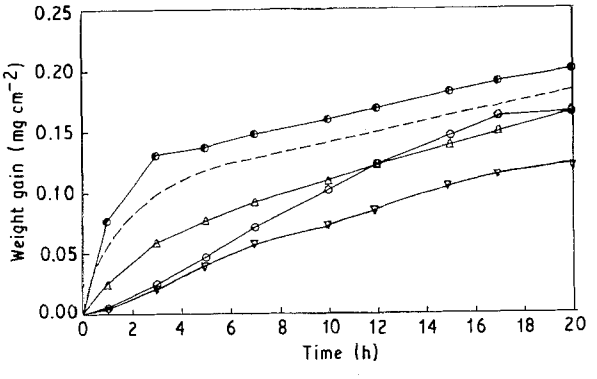

Figure 3 Mass gain per unit area versus time at 900 °C. (– – –) Ni_3Al (‖); (◐) B (4×10^{16}); (○) B (1.5×10^{17}); (△) B (‖) (1.5×10^{17}); (▽) Cr (2×10^{17}) + B (1.5×10^{17}).

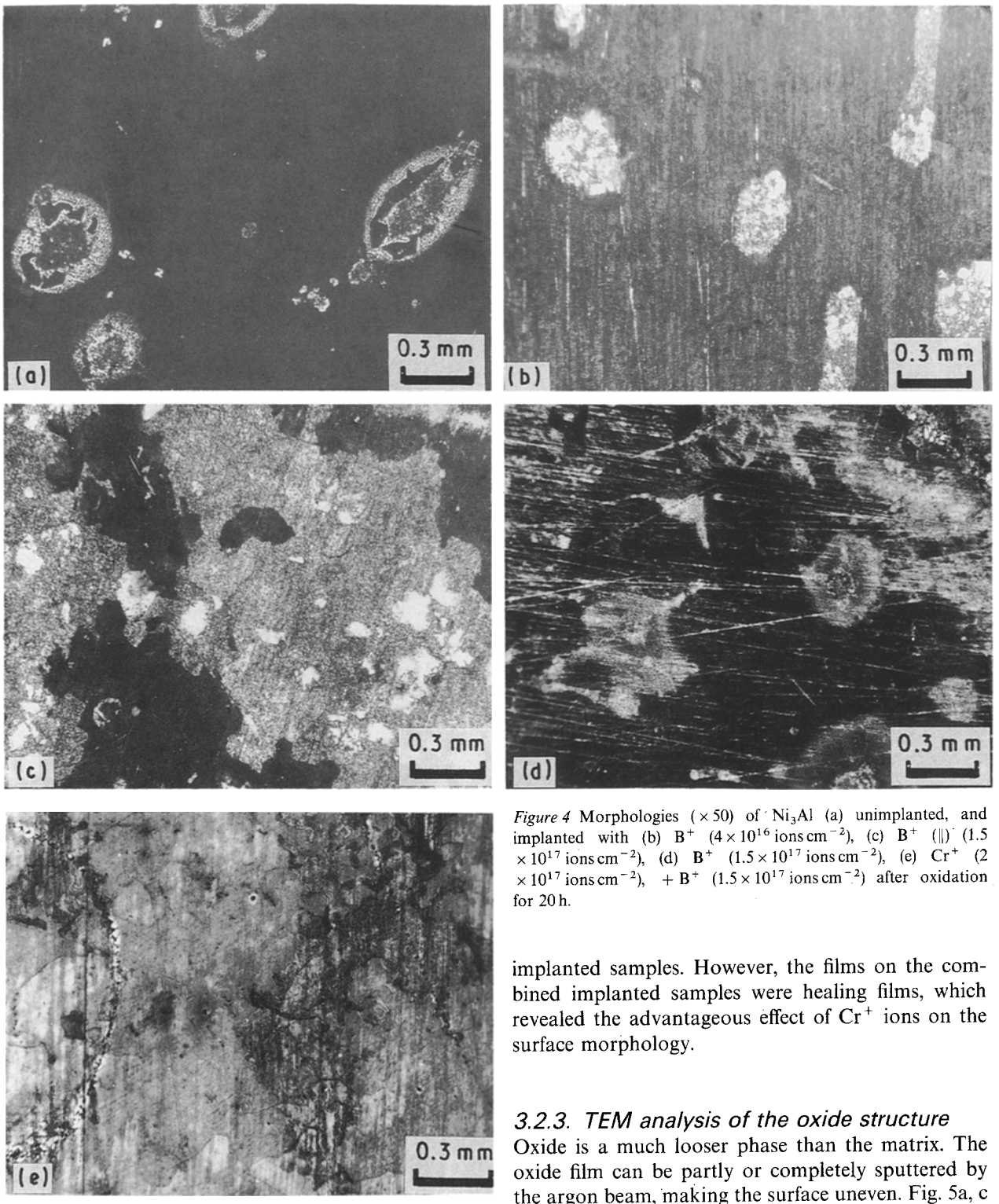

Figure 4 Morphologies (×50) of Ni_3Al (a) unimplanted, and implanted with (b) B^+ (4×10^{16} ions cm^{-2}), (c) B^+ (‖) (1.5×10^{17} ions cm^{-2}), (d) B^+ (1.5×10^{17} ions cm^{-2}), (e) Cr^+ (2×10^{17} ions cm^{-2}), + B^+ (1.5×10^{17} ions cm^{-2}) after oxidation for 20 h.

apparent change in oxidation kinetics, as shown in Fig. 3. The oxidation rates of the implanted samples were much lower compared with that of the unimplanted one. The higher the implanted dose, the better was the effect. Different orientations made no difference. The combined implanted sample exhibited the best improvement in the oxidation resistance.

3.2.2. Surface morphology of the oxides

An optical morphology observation of oxidized samples, as seen in Fig. 4, showed that boron implantation had no obvious effect on the surface morphology. Spallation occurred on both unimplanted and B^+-implanted samples. However, the films on the combined implanted samples were healing films, which revealed the advantageous effect of Cr^+ ions on the surface morphology.

3.2.3. TEM analysis of the oxide structure

Oxide is a much looser phase than the matrix. The oxide film can be partly or completely sputtered by the argon beam, making the surface uneven. Fig. 5a, c and e show the various oxide morphologies of B^+ implanted sample. Fig. 5b, d and g, which are identified as trigonal a-Al_2O_3, f c c NiO and hexagonal B_2O_3, are the corresponding SAD patterns of region in a, c and e, respectively. Both a-Al_2O_3 and NiO phases are fine-grained, but the B_2O_3 phase is comparatively larger.

3.2.4. Oxide structure analysis of combined implanted sample by SIMS

Secondary ion mass spectroscopy (SIMS) was used to analyse the oxide structure of the combined implanted sample. Argon ions were used as sputtering ions. Elemental profile distributions are shown in Fig. 6.

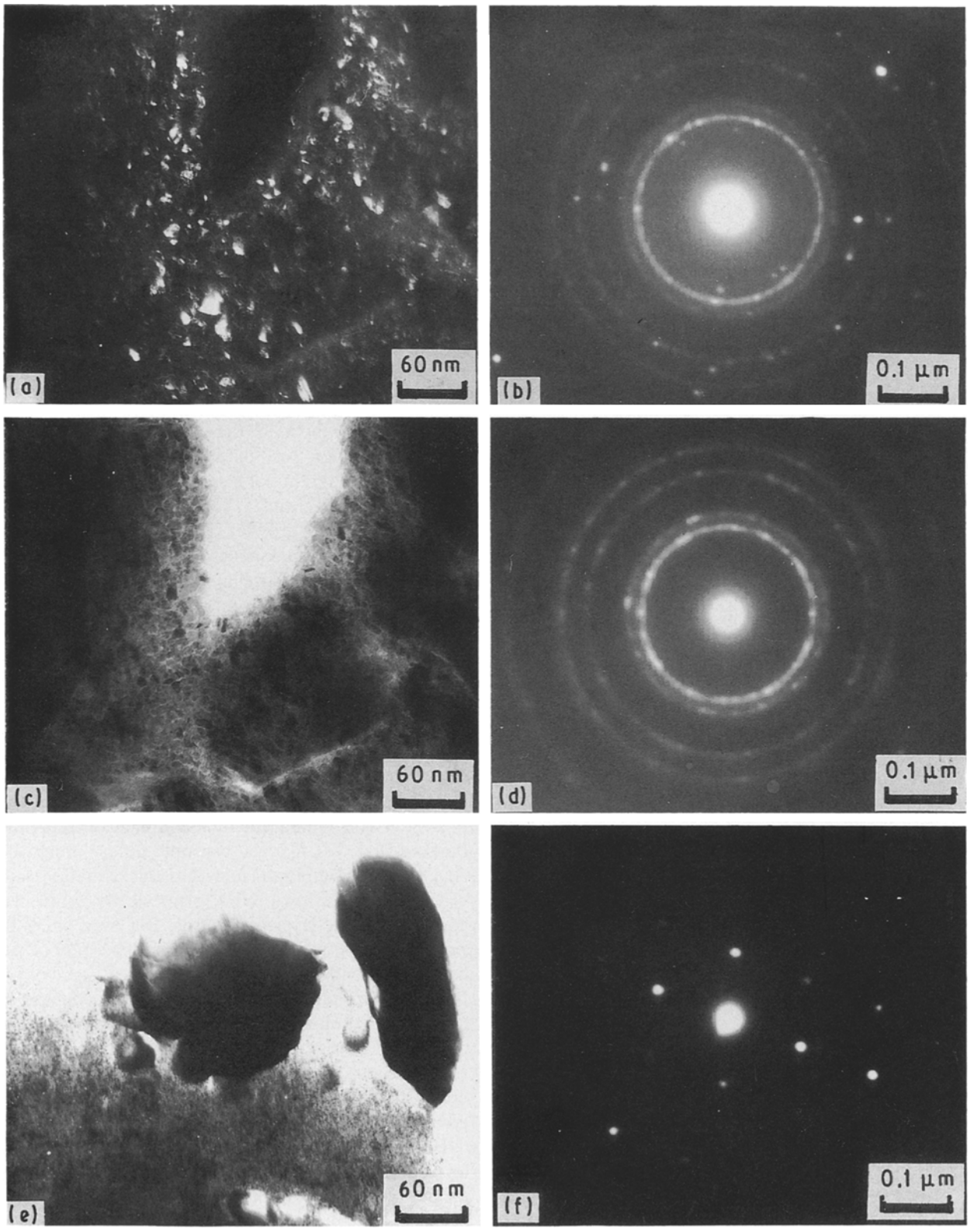

Figure 5 B^+-implanted Ni_3Al after oxidation, TEM (a) dark-field, (c, e) bright field images, and (b, d, f) corresponding SAD patterns.

Note that there is a nickel-depleted region at Point A.

4. Discussion

On implanting B^+ ions into Ni_3Al, no new phase was found in the alloy. This can be understood if we consider that boron atoms exist in the form of interstitial atoms in the crystal lattice.

The Gibbs' free energies of formation of the oxides show that NiO is less stable than a-Al_2O_3. However, the growth rates are in the ratio of $NiO:Al_2O_3 = 1:10^{-3}$–10^{-4} [3]. Both thermodynamics and kinetics influence the overall film development. NiO grows at a considerably faster rate. But, aluminium atoms have a higher affinity for oxygen than nickel, and form more stable oxides. Even though the relative free energies of formation of the oxides predict the

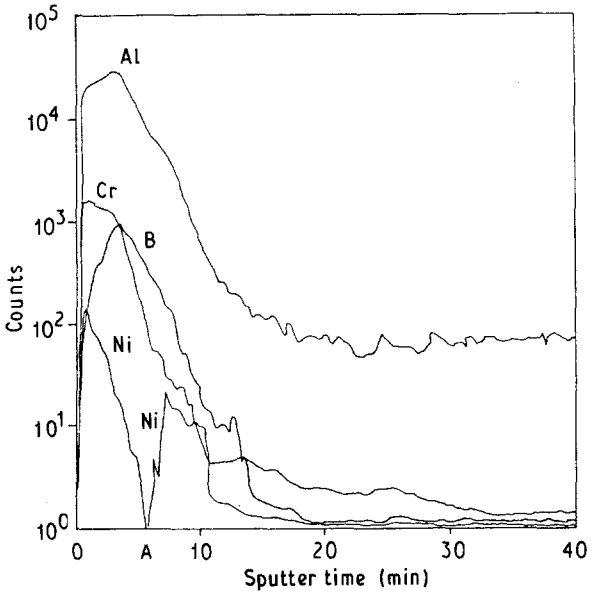

Figure 6 SIMS depth profiles of $Cr^+ + B^+$-implanted Ni_3Al after oxidation.

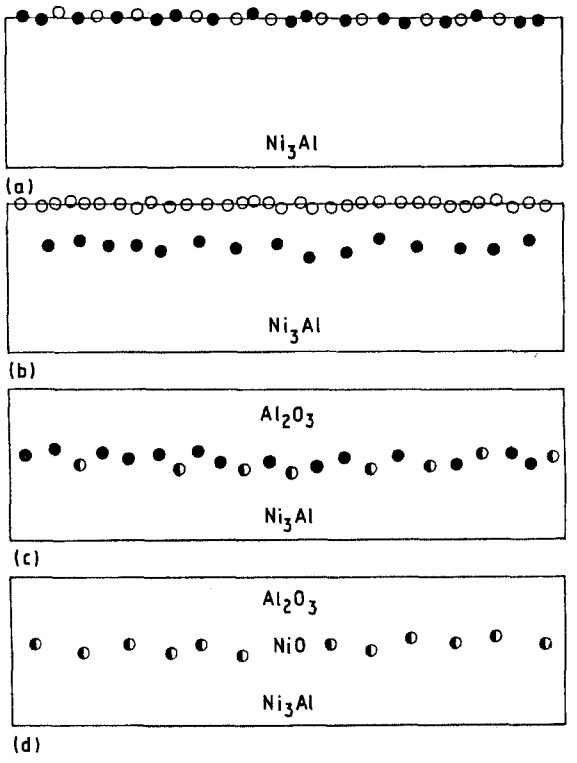

Figure 7 Schematic representation of progressive establishment of an oxide layer on B^+-implanted Ni_3Al. (○) NiO, (●) Al_2O_3, (◐) B_2O_3.

thermodynamically favoured oxide, they do not determine completely the nature of the transient oxide or of the steady-state scale.

The existing form of alumina is mainly determined by the content of aluminium in the alloy. Aluminium plays a critical role in the oxidation of γ′-strengthened superalloy. Pettit predicted [4] that when the content of aluminium is over 17 at %, the external Al_2O_3 scale would be maintained due to a sufficient supply of aluminium. So, in the high-temperature oxidation of Ni_3Al, aluminium atoms are selectively oxidized and form a continuous external oxide layer of Al_2O_3,

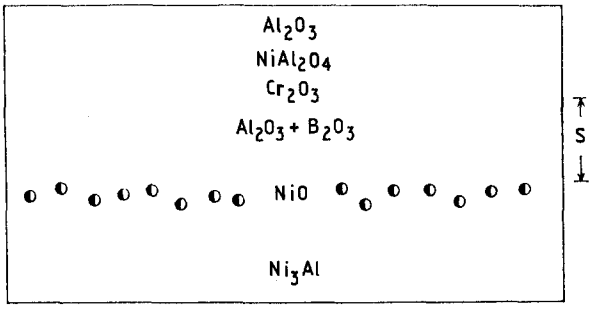

Figure 8 Schematic representation of the oxide layer on $Cr^+ + B^+$-implanted Ni_3Al. (◐) B_2O_3; S, nickel-depleted region.

which will suppress the further oxidation of the inner alloy.

Fig. 7 is a schematic diagram of the progressive establishment of the oxidation of B^+-implanted Ni_3Al. During the initial stage, nuclei of stable oxide phases, both NiO and a-Al_2O_3, are formed on the surface. The fastest growing phase, NiO, rapidly overgrows a-Al_2O_3 for kinetic reasons. Boron atoms diffuse to grain boundaries and defects at high temperature and form a space network. In Fig. 7b, NiO dissolves at its dissociation pressure and supplies oxygen due to its lower stability, which promote the oxidation of aluminium. When the oxygen diffuses outwards along grain boundaries and defects, boron atoms are oxidized into B_2O_3. This precipitated oxide curtails the short-circuit diffusion of oxygen. In Fig. 7c, a complete healing layer of a-Al_2O_3 is established. Finally, because of the formation of the protective Al_2O_3 film, the diffusion path of oxygen is blocked (Fig. 7d). Oxygen can only diffuse along the Al_2O_3 grain boundaries and thus the oxidation rate obviously slows down. NiO forms slowly below the complete Al_2O_3 layer afterwards. But even so, NiO will become the prominent oxide phase because of the highest content of nickel.

Chromium and boron exist at different depths in the combined implanted sample. Chromium is at the outer surface region and boron at the inner surface region because of their different atomic weights. They exert effects almost independently, which combine the advantages of both elements.

For a combined implanted sample, Cr_2O_3 is only formed at a certain depth due to the implantation. The formation of Cr_2O_3 improves the oxidation resistance of Ni_3Al, which can be proved by the mass-gain plot. We deduce from this that a protective Cr_2O_3 layer formed during oxidation. A solid state reaction occurs below the complete Al_2O_3 film and forms $NiAl_2O_4$ spinel [4]. According to the SIMS results, the oxide structure of the combined implanted sample after 20 h oxidation is as shown in Fig. 8. The nickel-depleted region can be explained by the fact that the contents of Cr_2O_3, Al_2O_3 and B_2O_3 are very high in this region. It is easy to see that the multiple obstacles for the inward diffusion of oxygen lead to the much lower oxidation rate, i.e. the combined implantation of chromium and boron ions can improve the oxidation resistance remarkably.

5. Conclusions

1. In the Cr^+ and B^+ combined sample, chromium atoms exist at the outer surface region and boron atoms exist in the inner surface region. Because the overlap region is very narrow, it can be considered that there are two independent implanted layers.

2. No evidence has been found that there is any new phase in boron-implanted Ni_3Al. Boron atoms possibly exist in the form of interstitial atoms in the crystal lattice because of the small atomic volumes.

3. On modification by boron implantation, the oxidation resistance of Ni_3Al is much improved: the higher the dose, the better the effect. Different orientations have no effect. The combined implanted sample has the best oxidation resistance.

4. During oxidation, the boron atoms diffuse to grain boundaries and defects and are oxidized to B_2O_3. The B_2O_3 particles curtail the short-circuit diffusion path of oxygen, which effectively improves the oxidation resistance.

5. Chromium and boron elements exist at different depths in the combined implanted sample. They exert effects almost independently, which combine the advantages of both elements and form multiple obstacles for the inward diffusion of oxygen. That is, the combined implantations of chromium and boron ions can improve the oxidation resistance remarkably.

Acknowledgements

This work was supported by the Chinese National Science Foundation. We are grateful for this support and to the Chinese Academy of Atomic Energy for the ion implantations.

References

1. K. K. AOKI and O. IZUMI, *J. Jpn Inst. Metals* **43** (1979) 1190.
2. N. S. STOLOFF, *Int. Metals Rev.* **34** (4) (1989) 1.
3. F. H. STOTT, *Mater. Sci. Technol.* **5** (1989) 734.
4. F. S. PETTIT, *Trans TMS-AIME* **239** (1967) 1296.

Received 2 September 1991
and accepted 24 July 1992